01/12/04-9:08 AM
Report No. LBNL 54277

Materials Sciences Division, Lawrence Berkeley National Laboratory, and
Department of Materials Science and Engineering,
University of California at Berkeley

FAILURE BY FRACTURE AND FATIGUE IN "NANO" AND "BIO" MATERIALS

R. O. Ritchie,[1,3] ***C. L. Muhlstein,***[2] ***and R. K. Nalla***[1]

[1]Materials Sciences Division, Lawrence Berkeley National Laboratory, and
Department of Materials Science and Engineering, University of California, Berkeley CA 94720

[2]Department of Materials Science and Engineering, The Pennsylvania State University, University Park, PA 16802

[3]*Corresponding author:* RORitchie@lbl.gov (R. O. Ritchie)
tel: (510) 486-5798; fax: (510) 486-4881

December 2003

submitted to *International Journal of JSME*

This work was supported by the Director, the Office of Science, Office of Basic Energy Sciences, Division of Materials Sciences and Engineering, of the U.S. Department of Energy under Contract No. DE-AC03-76SF00098 (for studies of silicon), and by National Institutes of Health under Grant No. P01DE09859 (for studies on mineralized tissue).

Corresponding author: Robert O. Ritchie, roritchie@lbl.gov

Failure by Fracture and Fatigue in "Nano" and "Bio" Materials

R. O. Ritchie[1], C. L. Muhlstein[1,2] and R. K. Nalla[1]

[1] *Materials Sciences Division, Lawrence Berkeley National Laboratory, and Department of Materials Science and Engineering, University of California, Berkeley, CA, USA*
[2] *currently at The Pennsylvania State University, University Park, PA, USA*

Abstract

The behavior of nanostructured materials/small-volume structures and biological/bio-implantable materials, so-called "nano" and "bio" materials, is currently much in vogue in materials science. One aspect of this field, which to date has received only limited attention, is their fracture and fatigue properties. In this paper, we examine two topics in this area, namely the premature fatigue failure of silicon-based micron-scale structures for microelectromechanical systems (MEMS), and the fracture properties of mineralized tissue, specifically human bone.

Key words: Fracture toughness, Fatigue, Polysilicon, Thin films, MEMS, Bone

Corresponding author: Robert O. Ritchie, roritchie@lbl.gov

1. INTRODUCTION

Materials scientists currently live in a world dominated by "buzz words" that define what is currently in favor and hence what is fundable and worthy of study. At present, the two of the most important words are "nano" and "bio", which respectively describe the areas of nanostructured materials/small-volume structures and biological/bio-implantable materials. With respect to the problems of fracture and fatigue, however, both areas still lack the sound understanding that we typically associate with traditional engineering materials and structures, and yet they clearly offer "fruitful ground" for fascinating new studies. This paper focuses briefly on two such topics, namely (i) the failure of "small-volume" structures for microelectromechanical systems (MEMS), specifically involving the high-cycle fatigue of micron-scale thin films of silicon, and (ii) the fatigue and fracture toughness properties of the mineralized tissues, specifically human bone, in simulated physiological environments.

With respect to the high-cycle fatigue of thin-film silicon, micron-scale structures of mono- and polycrystalline silicon have been found to be vulnerable to degradation by fatigue in ambient air and to fail after lives in excess of 10^{11} cycles at stresses as low as half the (single-cycle) fracture strength. Indeed, although bulk silicon is ostensibly immune to cyclic fatigue and subcritical crack growth, micron-scale films of silicon actually display "metal-like" stress-life (*S*/*N*) fatigue behavior. This phenomenon is of concern as most structures for MEMS fabricated from thin-film silicon are designed on the basis of the fracture strength, which will be non-conservative for predicting failure. Our experiments, however, have clarified the origin of this fatigue susceptibility of thin-film silicon. *S/N* fatigue testing, transmission electron microscopy, infrared microscopy and numerical models have been used to establish that the mechanism of such failure involves the sequential oxidation and environmentally-assisted crack growth of the native oxide layer, a process that is termed "reaction-layer fatigue". Only thin film/small volume silicon structures are prone to such failures as the critical crack size for catastrophic failure of the entire structure can be exceeded by a nano-scale crack solely within the native oxide layer. Methods to reduce this susceptibility, through the use of monolayer coatings, are described.

Turning to the fracture properties of "hard" mineralized tissue such as human bone, although there is substantial clinical interest in fracture resistance, little mechanistic information is available on how such materials derive their toughness and how they are specifically affected by fatigue. For example, the critical fracture event in human bone is widely believed to be locally strain-controlled, although no direct evidence has ever been offered to support this belief. In this paper, *in vitro* experiments are described involving a novel double-notched four-point bend geometry, which is designed to discern whether the onset of fracture is stress- or strain-controlled. Such experiments are further used to examine the interaction of cracks with the microstructure in bone in order to characterize the salient mechanisms of toughening. Additionally, *in vitro* fracture experiments are described in order to quantitatively assess the contributions of such mechanisms. It is found that the precursor fracture events are consistent with a strain-based mechanism, and that toughening is developed through a variety of extrinsic mechanisms, including crack bridging (from collagen fibrils and uncracked ligaments) and diffuse microcracking. Furthermore, the fracture toughness is found to rise linearly with crack extension (i.e., rising resistance- or R-curve behavior), and compliance-based experiments are used to identify that uncracked-ligament bridging is the dominant toughening mechanism responsible for such R-curve behavior.

2. FATIGUE OF "SMALL VOLUMES"

Silicon-based structural films remain the dominant material for MEMS because the micromachining technologies are readily adaptable from the microelectronics industry and are compatible with fabrication strategies for actuation and control integrated circuits. However, as noted above, the long-term durability of MEMS may be compromised by the susceptibility of thin-film silicon to premature failure by fatigue [1-10].

Fatigue in ductile materials results from cyclic plasticity characteristically involving alternating blunting and resharpening of a pre-existing crack tip as it advances [11,12]; in brittle materials where dislocation mobility is restricted, fatigue occurs by cycle-dependent degradation of the (extrinsic) toughening in the wake of the crack tip [11].[1] Silicon is a brittle material, with virtually no dislocation activity below ~500°C and no evidence of extrinsic toughening [13] or susceptibility to environmental cracking [14]; it should therefore not be prone to fatigue at room temperature. However, although there are no indications that bulk silicon is susceptible to fatigue failure, cyclically-stressed micron-scale films of silicon are known to fail in room air at stresses well below their fracture strength [1-10]. The mechanistic origins of this effect are described below.

2.1. Microstructure of micron-scale silicon films

The thin films examined were low-pressure chemical vapor deposited (LPCVD) n^+-type polycrystalline silicon, fabricated as 2-μm thick films using the MCNC/Cronos MUMPs™ process. Wafer curvature measurements indicated a compressive residual stress in the films of ~9 MPa. Secondary ion mass spectroscopy (SIMS) analysis revealed the presence of $\sim 2\times10^{18}$ $^{\text{atoms}}/_{\text{cm}^3}$ hydrogen, 1×10^{18} $^{\text{atoms}}/_{\text{cm}^3}$ oxygen, and 6×10^{17} $^{\text{atoms}}/_{\text{cm}^3}$ carbon [6]; in addition, 1×10^{19} $^{\text{atoms}}/_{\text{cm}^3}$ of phosphorous were detected from the phosphosilicate glass used for doping. The films, which were representative of those used throughout micromachining and MEMS research and production, had a Young's modulus of 163 GPa and a Poisson's ratio of 0.23. Fracture strengths typically ranged from 3 to 5 GPa, depending on loading condition, specimen size, and test technique, with a fracture toughness, K_c, of ~1 MPa√m [13].

The film microstructures had an equiaxed grain morphology (grain size of ~100 nm), with no strong texture, no segregation of O, C, P or N, or precipitation of secondary species in the films. Diffraction contrast imaging using transmission electron microscopy (TEM) revealed several types of lattice defects, including microtwins, stacking faults and Lomer-Cottrell dislocation locks.

2.2. Micron-scale fatigue testing

Fatigue life as a function of applied stress was determined using a notched cantilever-beam specimen within a micron-scale "on-chip" fatigue characterization structure (Fig. 1) [3,4]. Polysilicon samples were prepared by removing the sacrificial oxide layer in 49% HF for 2½ - 3 min, drying at 110ºC in air, and mounting in ceramic electronic packages. The notched beam specimen (~40 μm long, 19.5 μm wide, and 2 μm thick, with a 13 μm deep, 1 μm radiused notch), was attached to a large, perforated plate that served as a resonant mass. The mass and beam were electrostatically forced to resonate and the resulting motion measured capacitively. This generated fully-reversed, constant-amplitude, sinusoidal stresses at the notch, i.e., a load ratio of $R = -1$, that were controlled to

[1] Unlike *intrinsic* toughening which involves an increase in the inherent resistance to microstructural damage ahead of the crack tip, *extrinsic* toughening mechanisms act primarily behind the crack tip to "shield" the crack from the full applied driving force. Examples include transformation toughening and grain bridging in ceramics and fiber bridging in composites (e.g., [11]).

better than 1% precision. Specimens were cycled to failure at resonance with a frequency of ~40 kHz in ambient air (~25ºC, 30-50% relative humidity) at stress amplitudes ranging from 2 to 4 GPa, using the control scheme described in refs. [3,4].

The specimen compliance, computed from change in the natural frequency of the system [4,15], was monitored *in situ* to evaluate the evolution of damage in the sample from cracking and oxide formation. Experiments using an unnotched specimen have been used to demonstrate that changes in resonant frequency are a result of such damage and are not due to variations in temperature, relative humidity or accumulation of debris [6]. The relationship between stresses in the vicinity of the notch and its dynamic response was determined using finite-element modeling. Such methods were also used to evaluate the natural frequency, compliance, crack length, and stress-intensity factor, K, for structures containing cracks. The numerical models were constructed using a commercial software package (ANSYS v 5.7) [15].

2.3. Micron-scale stress-life fatigue

Stress-life (*S/N*) data for the polysilicon films are shown in Fig. 2a, based on a total of 28 specimens tested in room air [4]. The silicon films can be seen to display "metal-like" *S/N* behavior, with an endurance strength at 10^9 - 10^{10} cycles of roughly half the (single-cycle) fracture strength. Similar behavior has been seen in 20-μm thick films of single-crystal silicon cycled under identical conditions [3]. The change in resonant frequency of the specimens was monitored during testing to provide a measure of the specimen compliance. The frequency decreased (by up to 50 Hz in the long-life tests) before eventual specimen failure at the notch; indeed, using plane-stress finite element modal analyses with ANSYS [4,15], this was related to the stable growth of a crack (Fig. 2b). This analysis implies cracking occurring on length scales commensurate with the native oxide thickness; indeed, estimates of the crack length, plotted in Fig. 2b, reveal crack sizes less than 50 nm throughout the entire test.

SEM and TEM of failed specimens established that overload fracture in the films occurred by transgranular cleavage. Although SEM studies were inconclusive in discerning differences between these and the fatigue fractures, this was clearly evident in high-voltage (~1 MeV) TEM. Examination of fatigue and untested control samples revealed a stark difference in the native oxide at the notch root. In control samples, a ~30 nm thick layer of oxide was uniformly distributed over the sample surfaces (including the notch); in the fatigue samples, however, the oxide layer at the notch was a factor of 3 thicker (Fig. 3).

As *in situ*, high-resolution infrared (IR) imaging of the fatigue characterization structure revealed no changes in temperature greater than 1°C at the notch root during testing, the enhanced notch-root oxidation appeared to be mechanical in origin [9,10].

The precise nature of this effect is unclear, but may be related to such processes as stress-assisted diffusion and cracking within the notch oxide layer which permits the further ingress of moisture and continued oxidation in this region (e.g. [16]). Despite uncertainty in the origin of this layer, its role in thin-film silicon fatigue is far clearer. By interrupting fatigue specimens prior to failure and examining them with TEM, several small growing cracks (on the order of tens of nanometers in length) were observed within the native oxide at the notch root (Fig. 4). The size of these cracks was consistent with the compliance change predicted by finite-element modeling. Such cracking in the oxide layer is considered to be moisture-induced. Since the toughness of the SiO_2 (K_c ~ 0.8 MPa$\sqrt{m}$) is comparable to that of silicon (K_c ~ 1 MPa$\sqrt{m}$), the oxide should not crack prematurely. However, unlike silicon, amorphous SiO_2 is susceptible to environmentally-assisted cracking in moisture; in-

deed, the threshold stress intensity, K_{scc}, for such cracking is much less than K_c, i.e., $K_{scc} \sim 0.25$ MPa$\sqrt{m}$, in contrast to silicon where $K_{scc} \approx K_c$ [14]. Since no phase transformations or dislocation activity were detected, the fatigue of Si films in ambient air was deemed to be associated with environmentally-assisted cracking in the native oxide layer that has been thickened under cyclic loading (Fig. 5).

In situ measurements of the natural frequency during the fatigue test were used to determine the crack length and hence the crack-driving force at failure; this provides a measure of the fracture toughness, which was computed to be ~0.85 MPa$\sqrt{m}$, consistent with that of the native oxide [15]. However, it is important to note the relationship between the critical crack size at final failure, a_c, where $K = K_c$, and the thickness, h_o, of the SiO_2 layer. If critical crack sizes are estimated for the range of applied stresses of 2 to 4 GPa which caused failure in the present films after 10^5 to 10^{11} cycles, it is apparent that the critical crack sizes are less than 50 to 70 nm, i.e., comparable the observed oxide layer thicknesses (i.e., $a_c \leq h_o$). This indicates that the entire fatigue-crack initiation and propagation process and the onset of catastrophic (overload) failure all occur within the oxide layer.

2.4. "Reaction-layer" fatigue

As noted above, silicon *per se* is not expected to be susceptible to cyclic fatigue or stress-corrosion cracking. At ambient temperatures, there is no evidence of mobile dislocation activity in silicon [19], which could permit crack advance by crack-tip blunting and resharpening (as in a ductile material). The cyclic fatigue of brittle materials, conversely, is caused by a degradation in extrinsic toughening in the crack wake [11], which arises in ceramics from crack-tip shielding mechanisms such as grain bridging; under cyclic loading, fracturing and chipping of the bridges and frictional wear in the sliding grain boundaries lead to a deterioration in the potency of the bridging [11,17,18]. As this necessitates intergranular fracture, which is not seen in polysilicon, again we would expect little susceptibility to fatigue damage.

However, the fatigue susceptibility of thin-film silicon is associated with a conceptually different mechanism, that of sequential mechanically-induced oxidation and environmentally-assisted cracking of the surface layer of native oxide that forms upon reaction with the atmosphere, termed *reaction-layer fatigue* [9,10]. This mechanism can be observed experimentally as a continuous decrease in the specimen stiffness during fatigue loading (Fig. 2b, [4]), and can be visualized directly using TEM (Figs. 3,4). The native oxide, which initially forms on the exposed silicon surface, thickens in high stress regions during fatigue loading and becomes the site for moisture-induced cracks that grow stably in the oxide layer. The process repeats itself until a critical crack size is reached, whereupon the silicon itself fractures catastrophically. The rate-dependence of thin-film silicon fatigue is thus dictated by the cycle-dependent oxide thickening process and the time-dependent moisture-assisted subcritical crack growth in this oxide layer [10].

This mechanism provides an explanation as to why thin-film silicon is prone to fatigue failure, even though bulk silicon is not. This is because cracking in the nano-scale native oxide film would have a negligible effect on a macroscopic sample of silicon under load, since crack sizes in the oxide could never reach critical size. In contrast, with thin films where the surface-to-volume ratio is far larger such that the oxide layer represents a large proportion of the sample, cracks within the oxide are readily able to exceed critical size and thus can cause failure of the entire silicon component.

An obvious test of this mechanism is to fatigue in an environment where the oxide cannot form. This was achieved through the use of coatings to suppress the formation of the native oxide. Accordingly, specific specimens were coated after HF release with a hydrophobic monolayer of alkene-based

1-octadecene ($C_{16}H_{33}CH =CH_2$) [20], which bonds directly to the H-terminated Si atoms on the surface such that no oxide can form (Fig. 6a). Initial results [10] on such SAM-coated films do show fatigue lifetimes that are far less affected by cyclic stresses (Fig. 6b), thereby providing support for the proposed reaction-layer mechanism of thin-film silicon fatigue.

3. FRACTURE OF BIOMATERIALS

Similar to the problem of small volume structures, biomaterials also represent an area where there is only limited understanding of mechanical behavior and its mechanistic origins. For example, the realization that bone mineral density alone cannot explain the therapeutic benefits of anti-resorptive agents in treating osteoporosis [21] has reemphasized the necessity of understanding how factors other than bone mineral density control fracture. Much of this renewed emphasis is being focused on bone "quality", where quality is used to describe mechanical characteristics of the tissue, which encompasses properties like elastic modulus, strength, and toughness. Though there have been many studies on this issue, specifically in terms of how the mechanical properties might vary with age and other related factors, only a few of these studies have addressed these properties within the context of microstructure of bone. Indeed, human bone has a complex multi-hierarchical microstructure that can be considered at several dimensional scales [22,23]. At the shortest length-scale, it is composed of type-I mineralized collagen fibers (up to 15 μm in length, 50-70 nm in diameter) bound and impregnated with carbonated apatite nanocrystals (tens of nm in length and width, 2-3 nm in thickness) [22]. These fibers are further organized at a microstructural length-scale into a lamellar structure with roughly orthogonal orientations of adjacent lamellae (3-7 μm thick) [23]. Permeating this lamellar structure are the secondary osteons [24][2[] (up to 200-300 μm diameter): large vascular channels (up to 50-90 μm diameter) oriented roughly in the growth direction of the bone and surrounded by circumferential lamellar rings, with so-called "cement lines" at the outer boundary. The difficulty in understanding the mechanisms of fracture in bone clearly lies in determining the relative importance of these microstructural hierarchies on crack initiation, subsequent crack propagation and consequent unstable fracture, and in separating their effects on the critical fracture events. Such an understanding is of vital importance from the perspective of developing a realistic framework for fracture risk assessment, and for determining how its increasing propensity for fracture with age can be prevented.

One pertinent feature of the failure of biomaterials such as bone is a definition of the critical microstructural steps involved in the development of fracture. Although micromechanical models incorporating such local failure criteria have been developed for metallic and ceramic materials [25,26], few such models exist for biological materials. In fact, there is no proof to support the widely held belief that fracture in bone is locally strain-controlled [27,28]. Below, a novel series of *in vitro* experiments is described to obtain such evidence using a double-notch-bend geometry designed to shed light on the nature of the critical failure events in bone. In addition, how the propagating crack interacts with the bone microstructure is examined to provide some mechanistic understanding of fracture and to define how properties vary with orientation.

3.1. Double-notch, four-point bend testing

A vital distinction in the definition of the local (precursor) fracture events that cause macroscopic failure is whether they are locally *stress*- or *strain-controlled*. Brittle fracture is invariably stress-controlled, for example in structural steels at low temperatures where cleavage fracture is instigated by the precursor cracking of carbide particles or inclusions [25,26]. Ductile fracture, conversely, is strain-controlled, as in the same steels at higher temperatures where the fracture process involves ductile tearing between such particles or inclusions (with a significant increase in toughness) [26]. Bone fracture is widely regarded as strain-controlled; indeed, most theoretical descriptions of its

mechanical behavior assume this to be the case [27]. However, experimental evidence for this assertion has never been obtained.

To investigate this distinction, a double-notched four-point bend test was used, consisting of a rectangular bar containing two nominally identical rounded notches (root radius ~200 μm) subjected to four-point bending. The basis of the test is that with a rounded notch in the presence of some degree of inelasticity or yielding, although the maximum local strains are located *at* the root of the notch [26], the relaxation of stresses in the inelastic ("yielded") zone surrounding the notch results in the maximum local stresses being located some distance *ahead* of the notch, close to the elastic-inelastic interface [29] (Fig. 7a). Since the two notches experience the same bending moment, when one notch breaks, the other is "frozen" at a point immediately preceding fracture. Examination of the area in the vicinity of the unfractured notch thus reveals the nature of the *local* fracture event at the onset of failure (area indicated in Fig. 7b "*After fracture*" illustration).

It is appreciated that "yielding" in bone cannot be simply related to shear-driven plasticity, e.g., in metals, for which the notch-field solutions in Fig. 7a were explicitly derived. Indeed, the precise nature of the inelastic constitutive behavior of bone is not known, but clearly involves diffuse microcracking damage and plasticity in the collagen fibrils, which would be sensitive to both tensile and shear stresses (somewhat akin to pressure-dependent yielding in polymers). Despite this, most theoretical models for both deformation [30] and fracture [31] in bone utilize the Mises criterion, which was derived for pressure-insensitive plasticity. Our recent studies using a microcracking model for inelastic deformation have in fact shown that the notch fields for an idealized bone-like material are qualitatively identical to those for pressure-insensitive shear-driven plasticity [32].

Results for tests in 37°C Hanks' Balanced Salt Solution (HBSS) are given in Fig. 8, and show the unbroken notches in specimens of a cadaveric human humerus. The extremely small (<5 μm) size of the precursor cracks that were imaged in all orientations (Fig. 7c) leaves little doubt that crack initiation is *at* the notch and not ahead of it (Fig. 8). Moreover, assuming a plasticity-based criterion, numerical analysis of the specimens at maximum load where the nominal elastic bending stress, σ_{nom}, at the notch was in the 40-100 MPa range (ratio of nominal stress to yield stress of σ_{nom}/σ_y ~0.53-1.33), suggests that the tensile stresses should peak well ahead of the notch (at ~100-360 μm ahead of the notch tip*, i.e.*, at a distance of 0.5-1.2 times the notch-root radius). As absolutely no evidence of any precursor cracking was found in this region and all initial cracks were detected exactly at the notch root, our observations are consistent with fracture in bone being associated with a strain-based criterion. Similar studies with identical results have been performed for dentin, the principal constituent of human teeth [33].

3.2. Mechanisms of fracture in bone

Insights into the mechanisms of fracture in bone and how it derives its toughness can also be obtained from these experiments. Various toughening mechanisms have been proposed for bone. At large length-scales, the generation of "microdamage" from microcracking (small cracks of up to hundreds of micrometers in size) has been suggested as a source of toughening, specifically via crack-tip shielding [34,35]. In addition, the cement lines (at the secondary osteons boundaries) and the interlamellar boundaries are believed to provide weak interfaces to deflect the crack path and accordingly increase the toughness [36]. More recently, a role of collagen fibrils has been postulated [37], with fiber bridging proposed as a possible toughening mechanism [38]. Indeed, toughening at the fibrillar level would explain the apparent correlation of toughness with collagen denaturation, which appears to weaken bone, and cross-links, which appear to increase its toughness [39], although it is probable that many of these mechanisms operate in concert.

Characterization: Scanning electron micrographs of the *in vitro* fracture paths in human bone, specifically indicating how the crack interacts with the microstructure, are shown in Fig. 9. Fig. 9a shows a roughly 1-mm-long crack propagating out of the notch in the "anti-plane longitudinal" (medial-lateral) orientation, i.e., the plane of the crack and the crack front are nominally parallel to the long axis of the osteons. It is apparent that at this scale of observation, the most recognizable features of the microstructure, the Haversian canals with their concentric lamellar rings, do not have a major influence on the path taken by the growing crack. Investigation of the near-tip region of this crack, however, shown by the white circle, revealed evidence of so-called *uncracked-ligament bridging*, as indicated by the white arrow in Fig. 9b. This is an extrinsic toughening mechanism involving two-dimensional uncracked regions along the crack path that can bridge the crack on opening; it is commonly seen in metal-matrix composites [40] and intermetallics such as γ-based TiAl [41]. Such bridging, however, is more prominent in the "in-plane longitudinal" (proximal-distal) orientation, as shown by the white arrow in Fig. 8b, where evidence of microcracking is also apparent near the crack. This can also lead to extrinsic toughening through its effect in creating dilation and reducing the modulus in the region surrounding the crack. For the "anti-plane longitudinal" orientation, a third mechanism of toughening in bone can be seen in Fig. 9c in the form of crack bridging by the collagen fibrils (Fig. 9c).

However, for the "transverse" specimen orientations, where the osteons run along the specimen length, a much stronger influence of the underlying microstructure was observed on the crack path. Crack initiation and initial crack growth out of the notch was not in the direction normal to the maximum tensile stress, but rather in the direction of the osteons (Figs. 8d, 9d), consistent with the suggestion [36] that the osteonal cement lines, that are the interface between the osteonal system and the surrounding matrix, can provide a weak path for the propagation of the crack (Fig. 9d). The resulting large out-of-plane crack deflections can lead to substantial toughening (as estimated below) and must be considered as a leading factor associated with the marked anisotropy in the fracture properties of cortical bone.

Quantification and verification: Such notions on the mechanisms of toughening in bone and how they vary with orientation are consistent with *in vitro* fracture toughness measurements in 37°C HBSS. Using fatigue precracked bend samples, fracture toughness values of K_c = 5.33(±0.41) MPa√m were measured for the transverse orientation, as compared to 2.21(±0.18) MPa√m for anti-plane longitudinal orientation and 3.53(±0.13) MPa√m for the in-plane longitudinal orientation.

These observations and measurements can be verified by experiment and theory (as discussed in the next section). The toughening effect seen in the anti-plane longitudinal orientation can be assoicated with crack bridging by uncracked ligaments (and collagen fibrils) (Figs. 8b, 9a,b), although such micrographs alone are not definitive proof. To provide verification of a bridging effect, measurements of the elastic compliance (inverse stiffness) of the cracked specimen in 37°C HBSS were compared to those made after subsequent machining out the wake of the crack (which removes the bridging elements). The latter measurements were then verified by showing that they were identical to the theoretical compliance of a traction-free crack of the same size. Such procedures have been documented as a means of quantifying the role of such crack bridging in ceramic materials [42]. Results for the anti-plane longitudinal orientation are shown in Fig. 10 and clearly indicate that the crack in the specimen has a lower compliance than a traction-free crack of identical length. Such results provide definitive proof that cracks in human bone are bridged.

Such measurements also permit the approximate quantification of the effect of such bridging on the toughening of bone from the difference between the two curves at maximum load; this gives the additional load sustained at the load-line, P_{br}~1.5 N, to overcome the effect of the "bridges". For the

present geometry, this value of the bridging load, P_{br}, can be equated to a bridging stress intensity, K_{br}. Calculations of K_{br}, which represent an extrinsic contribution to the fracture toughness, yielded values of ~0.5 MPa√m, i.e., they provide an ~25% elevation in K_c for this orientation. This definitive verification of the contribution of bridging to the toughening of bone implies that the use of a single-value fracture toughness is somewhat specious. Indeed, the fracture resistance can be expected to evolve with crack extension, promoting stable crack growth and requiring a resistance-curve (R-curve) fracture-mechanics approach [43].

3.3. Resistance-curve behavior in bone

R-curves are necessary to describe the fracture resistance of materials toughened by crack-tip shielding, i.e., by extrinsic toughening mechanisms such as crack bridging, constrained microcracking, or *in situ* phase transformations, which develop in the crack wake as the crack extends[e.g., 11]. In such instances, crack extension commences at a *crack-initiation toughness*, K_o, while sustaining further crack extension requires higher driving forces until typically a "plateau" or steady-state toughness is reached. The corresponding slope of the R-curve can be considered as measure of the *crack-growth toughness*.

The R-curve behavior of bone is shown in Fig. 11 based on the results of six compact-tension, C(T), specimens, machined from the mid-diaphysal sections of the humeri of two donors (34-year old female, 37-year old male) in the "in-plane longitudinal" (proximal-distal) orientation with the nominal crack-growth direction along the proximal-distal direction of the humerus, i.e., parallel to the long axis of the osteons (and hence, the humerus). Such R-curves evaluate the resistance to fracture in terms of the stress intensity, K, as a function of crack extension, Δa, under a monotonically increasing driving force. They were conducted in 20-40% relative humidity, ambient air with the specimens being continuously irrigated with HBSS and loaded in displacement control at a loading rate ~ 0.015 mm/s. The onset of cracking was determined by a drop in load, or non-linearity in the load-displacement curve, at which point, the sample was unloaded by 10-20% of the peak load to record the sample load-line compliance at the new crack length using a linear variable-displacement transducer (LVDT) mounted in the load frame. This process was repeated at regular intervals until the end of the test, at which point the compliance and loading data were analyzed to determine fracture resistance, K_R, as a function of crack extension, Δa. Crack lengths, a, were calculated from the compliance data obtained during the test using standard C(T) load-line compliance calibrations [44].

The resulting R-curves for hydrated cortical bone, shown in Fig. 11, reveal an average crack-initiation toughness, K_o, of 2.06 (S.D. = 0.2) MPa√m with the R-curves monotonically rising with a mean slope of 0.39 (S.D. = 0.09) MPa√m/mm). Such tests also allow for stable crack extension, again making it possible to directly observe the relevant toughening mechanisms and their relationship to the salient features of the microstructure. One effective means to do the latter is to use x-ray computed tomography which permits imaging of the crack path through the microstructure, either in two-dimensions in slices through the bone or in full three-dimensional reconstructions. This is done in Fig. 12, where the discontinuous nature of the crack path in the optical micrograph and the two-dimensional tomographic reconstructions in Fig. 12a indicates extensive formation of uncracked ligaments (indicated by white arrows) behind the crack tip and consequent "out-of-plane" deflection of the crack. On the sample surface, such ligaments are often as large as hundreds of micrometers in size and consequently they appear to be far more potent that bridging by individual collagen fibers. In Fig. 12b, a three-dimensional reconstruction for a section of a similar crack is shown. For both two-dimensional and three-dimensional tomography that the crack does not penetrate the osteon at any stage - the Haversian canal (and the surrounding lamellar structure) of the osteon seem totally ineffective in deflecting the crack from its path. Indeed, the path taken by the crack for this orienta-

tion appears to be totally dictated by the *interface* of the osteonal system with the surrounding matrix, *i.e.* the cement line, where the mineral content is locally higher.

Although it is not possible experimentally to separate out the relative contributions to bridging from the uncracked ligaments or the collagen fibrils, this distinction ca be achieved can be deduced from theoretical models for the two bridging mechanisms. Theoretical estimates of ligament bridging based on a limiting crack-opening approach [40] can be made using:

$$K_{br} = -f_{ul}K_I\,[(1+l_{ul}/rb)^{1/2} - 1] \,/\, [1 - f_{ul} + f_{ul}(1+l_{ul}/rb)^{1/2}] \quad , \tag{1}$$

where f_{ul} is the area fraction of bridging ligaments on the crack plane (~0.45), from crack path observations), K_I is the applied (far-field) stress intensity (~4.5 MPa$\sqrt{m}$), l_{ul} is the bridging zone size (~5 mm), r is a rotational factor (0.20-0.47) and b is the length of the remaining uncracked region ahead of the crack. Substituting typical values for these parameters, toughening of the order of K_{br} ~ 1-1.6 MPa$\sqrt{m}$ can be obtained. For toughening associated with bridging by the collagen fibrils, the uniform traction Dugdale zone model [45] can be employed to obtain an estimate of the resulting decrease in the stress intensity, K_b^f, due to "fiber-bridging", viz:

$$K_b^f = 2\sigma_b f_f (2l_f/\pi)^{1/2} \quad , \tag{2}$$

where σ_b is the normal bridging stress on the fibrils (~100 MPa), f_f is the effective area fraction of the collagen fibrils active on the crack plane (~0.15, from crack path observations), and l_f is the bridging-zone length (~10 μm, from crack path observations). Using these estimates, a value of K_b^f~0.07 MPa$\sqrt{m}$ can be obtained, suggesting that uncracked-ligament bridging provides a more significant contribution to the toughness of bone than bridging by individual collagen fibers. However, at smaller dimensions, collagen fibral bridging may still be important for individual small cracks on the order of microstructural size-scales.

In summary, direct experimental evidence has been presented in support of a *strain-controlled* fracture mechanism in bone. In addition, a series of extrinsic toughening mechanisms in bone have been identified (including crack bridging by uncracked ligaments and collagen fibrils, crack deflection, and microcracking), based on microscopic observations of the interaction of the crack path with the underlying microstructure. Based on these observations, experimental compliance measurements, and theoretical estimates for the toughening contributions of the mechanisms, the anisotropy in the fracture toughness of bone with orientation can be understood; specifically, we find a smaller (but finite) contribution to the toughening in the (anti-plane) longitudinal orientation due to crack bridging as compared to the larger contribution from crack deflection in the transverse orientation. It is believed that the results presented here are critical steps to the understanding of structure-function relationships in bone and can form the basis for a physically-based micro-mechanistic understanding of the fracture and failure of human cortical bone from a fracture-mechanics perspective.

To eliminate the added complexity introduced by aging-related changes, the results described above have been largely restricted to a rather narrow donor age group (34-41 years). There are a large number of studies in archival literature that have looked at age-related issues in the mechanical properties of bone (e.g., [46,47]), and have suggested a significant deterioration of the fracture toughness with age. In particular, aging has been associated with lowered collagen network integrity, with resultant reduction in the toughness [47], presumably due to poorer quality uncracked-ligament bridges being formed. Also, it has been suggested that remodeling induced by increasing microdamage with aging [48] leads to an increase in the difference in properties of the matrix (primary lamellar bone) and the secondary osteons, implying a stronger role for the cement lines and a reduc-

tion in the toughness . Clearly, further investigations are needed to assess how such changes affect the microstructure of bone at various levels, and their resultant effect on the mechanisms of toughening. Such an approach is fundamental to furthering our understanding of effect of aging on the fracture properties of mineralized tissues.

However, the simple materials science experiments described clearly show that the local criterion for fracture in human cortical bone is consistent with a *strain-based* criterion. It is believed that this is the first direct *experimental* evidence for the validity of the assumption of a strain-based criterion, which has been widely used in theoretical models of the mechanical behaviour of bone. In addition, the marked anisotropy in the toughness properties and the rising resistance-curve behavior of bone has been rationalized in terms of extrinsic toughening mechanisms induced by specific features in the microstructure. These results are of interest in that they form the basis of physically-based micro-mechanistic understanding of the fracture and failure of human cortical bone, which will have a strong bearing on the question of "bone quality" and how it degrades with age.

4. CONCLUSIONS

In this paper, we have attempted to show how novel materials science experiments and simple theoretical considerations can shed light on the mechanisms of fatigue and fracture in "small-volume" structures associated with silicon MEMS and in biological materials such as human bone. We believe that the materials scientist and engineer can play a major role both the "nano" and "bio" materials arenas, as there is both a need for sound engineering data and mechanistic understanding. Perhaps even more important is that for both MEMS and biological implants/devices, physically-based life-prediction analyses are sadly lacking, and this makes the realistic evaluation of the durability and reliability of these components and structures uncertain. It is clear that this represents an ideal future challenge for the materials and bioengineering communities.

ACKNOWLEDGMENTS

This work was supported by the Director, the Office of Science, Office of Basic Energy Sciences, Division of Materials Sciences and Engineering, of the U.S. Department of Energy under Contract No. DE-AC03-76SF00098 (for studies of silicon), and by National Institutes of Health under Grant No. P01DE09859 (for studies on mineralized tissue). Special thanks are due to Drs. John Kinney, Jay Kruzic, Roya Maboudian, James Stölken, Christian Puttlitz, and in particular Eric Stach for their collaboration with us on these studies.

REFERENCES

1. J.A. Connally and S.B. Brown, Science, 256 (1992), pp. 1537-1539.
2. S.B. Brown, W. Van Arsdell and C.L. Muhlstein, Proc. Int Solid State Sensors and Actuators Conf. (Transducers '97), ed. S. Senturia, IEEE (1997), pp. 591-593.
3. C.L. Muhlstein, S.B. Brown and R.O. Ritchie, JMEMS, 10 (2001), pp. 593-600.
4. C.L. Muhlstein, S.B. Brown and R.O. Ritchie, Sensors and Actuators A, 94 (2001), pp. 177-188.
5. H. Kahn, R. Ballarini, R. L. Mullenand A. H. Heuer, Proc. Roy. Soc. A, 455 (1999), pp. 3807-3823.
6. W.W. Van Arsdell and S.B. Brown, JMEMS, 8 (1999), pp. 319-27.
7. K. Komai, K. Minoshima and S. Inoue, Micros. Tech., 5 (1998), pp. 30-37.
8. S.M. Allameh, B. Gally, S. Brown and W. O. Soboyejo, Materials Science of MEMS Devices III, ed. H. Kahn, *et al*., MRS, 2000, pp. EE2.3.1-EE2.3.6.

9. C.L.Muhlstein, E.A. Stach and R.O. Ritchie, Appl. Phys. Let., 80 (2002), pp. 1532-1534.
10. C.L.Muhlstein, E.A. Stach and R.O. Ritchie, Acta Mater., 50 (2002), pp. 3579-3595.
11. R.O. Ritchie, Int. J. Fract., 100 (1999), pp. 55-83.
12. S. Suresh, Fatigue of Materials, 2nd ed., Cambridge University Press, Cambridge, UK (1998).
13. H. Kahn, N. Tayebi, R. Ballarini, R.L. Mullen and A.H. Heuer, Transducers '99: 10th Int. Conf. Solid State Sens. & Actuat., Elsevier, (1999), pp. 274-280.
14. B.R. Lawn, D.B. Marshall and P. Chantikul, J. Mater. Sci., 16 (1981), pp. 1769-1775.
15. C.L. Muhlstein, R.T. Howe and R.O. Ritchie, Mech. Mater., 36 (2004). Pp. 13-33.
16. A. Fargeix and G. Ghibaudo, J. Appl. Phys., 56 (1984), pp. 589-591.
17. S. Lathabai, J. Rödel, and B.R. Lawn, J. Am. Ceram. Soc., 74 (1991), pp. 1340-1348.
18. R.H. Dauskardt, Acta Metal. Mater., 41 (1993), pp. 2765-2781.
19. B.R. Lawn, B.J. Hockey and S.M. Wiederhorn, J. Mater. Sci., 15 (1980), p. 12.
20. W.R. Ashurst, C. Yau, C. Carraro, R. Maboudian, and M.T. Dugger, JMEMS, 10 (2001), pp. 41-49.
21. R.P. Heaney, Bone, 33 (2003), pp. 457-465.
22. J.Y. Rho, L. Kuhn-Spearing and P. Zioupos, Med. Eng. Phys., 20 (1998), pp. 92-102.
23. S. Weiner and H.D. Wagner, Ann. Rev. Mater. Sci., 28 (1998), pp. 271-298.
24. J.D. Currey, J. Biomech., 15 (1982), p. 717.
25. R.O. Ritchie, J.F. Knott and J.R. Rice, J. Mech. Phys. Solids, 21 (1973), pp. 395-410.
26. R. O. Ritchie, W.L. Server and R.A. Wullaert, Metall. Trans. A, 10A (1979), pp. 1557-1570.
27. O.C. Yeh and T.M. Keaveny, J. Orthopaed. Res., 19 (2001), pp. 1001-1007.
28. J.H. Keyak and S.A. Rossi, J. Biomech., 33 (2000), pp. 209-214.
29. J.R. Griffiths and D.R.J. Owen, J. Mech. Phys. Solids, 19 (1971), pp. 419-431.
30. P. Zioupos, J.D. Currey, M.S. Mirza and D.C. Barton, Philos. Trans. R. Soc. Lond. B. Biol. Sci., 347 (1995), pp. 383-396.
31. J.C. Lotz, E.J. Cheal and W.C. Hayes, J. Biomech. Eng., 113 (1991), pp. 353-360.
32. R.K. Nalla, J.S. Stölken, J.H. Kinney and R.O. Ritchie, J. Biomech., (2003), in review.
33. R.K. Nalla, J.H. Kinney and R.O. Ritchie, J. Biomed. Mater. Res., 67A (2003), pp. 484-495.
34. G.P. Parsamian and T.L. Norman, J. Mater. Sci.: Mater. Med., 12 (2001), pp. 779-783.
35. D. Vashishth, K.E. Tanner and W. Bonfield, J. Biomech., 33 (2000), pp. 1169-1174.
36. Y.N. Yeni and T.L. Norman, J. Biomed. Mater. Res., 51 (2000), pp. 504-509.
37. X. Wang, R.A. Bank, J.M. Tekoppele and C.M. Agrawal, J. Orthopaed. Res., 19 (2001), pp. 1021-1026.
38. Y.N. Yeni and D.P. Fyhrie, Proc Bioeng. Conf. BED 50, ASME, New York, NY, (2001), pp. 293-294.
39. D.B. Burr, Bone, 31 (2002), pp. 8-11.
40. J.H. Shang and R.O. Ritchie, Metall. Trans. A, 20A (1989), pp. 897-908.
41. J.P. Campbell, K.T. Venkateswara Rao and R.O. Ritchie, Metall. Mater. Trans. A, 30A (1999), pp. 563-577.
42. J.J. Kruzic, R.M. Cannon, R.O. Ritchie, J. Am. Ceramic Soc., 87 (2004).
43. J.F. Knott, Fundamentals of fracture mechanics, Butterworth & Co. (Publishers) Ltd.. London, U.K., (1976).
44. A. Saxena and S.J. Hudak, Int. J. Fract., 14 (1978), pp. 453-468.
45. A.G. Evans and R.M. McMeeking, Acta Metall., 34 (1986), pp. 2435-2441.
46. P. Zioupos and J.D. Currey, Bone, 22 (1998), pp. 57-66.
47. X. Wang, X. Shen, X. Li and C.M. Agrawal, Bone, 31 (2002), pp. 1-7.
48. T.C. Lee, A . Staines and D. Taylor, J. Anat., 201 (2002), pp. 437-446.

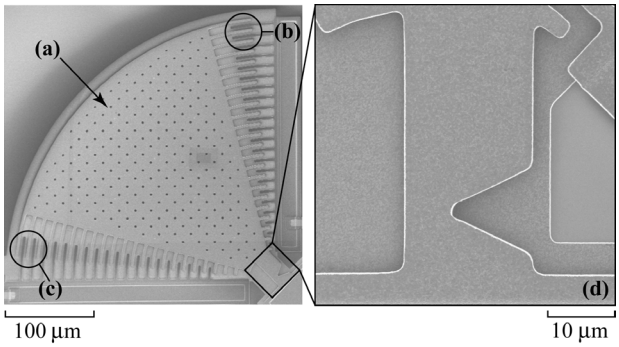

Fig. 1. SEM of the fatigue test structure, showing the (a) mass, (b) comb drive actuator, (c) capacitive displacement sensor, and (d) notched cantilever beam specimen.

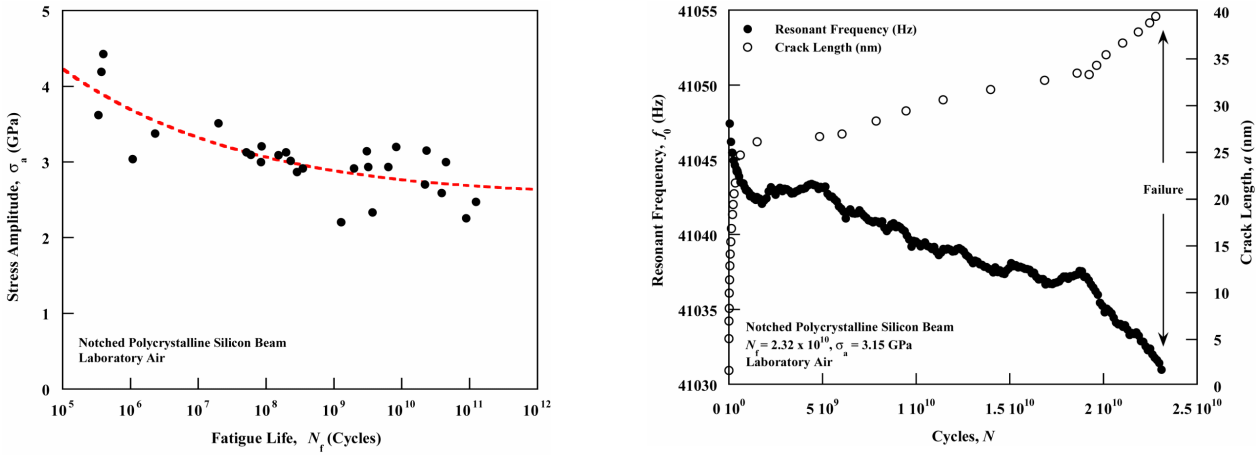

Fig. 2. (a) Stress-life curves for 2 µm-thick polysilicon at 40 kHz in moist air at R = -1. (b) *In situ* damage accumulation as a decrease in resonant frequency, f_{crack}, with time, with corresponding calculated increase in crack length, a.

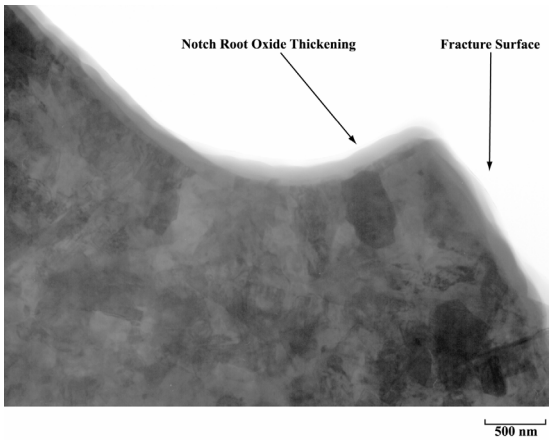

Fig. 3. High voltage (0.8 MeV) TEM image of the notch region in an unthinned polysilicon fatigue test sample, showing enhanced oxidation at the notch root after fatigue cycling.

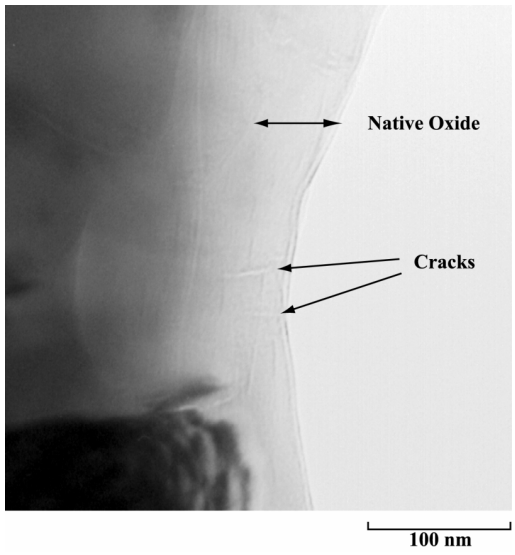

Fig. 4. High voltage (0.8 MeV) TEM image of the notch region in an unthinned polysilicon fatigue sample, showing ~50 nm long stable cracks in the native oxide layer formed during cyclic loading.

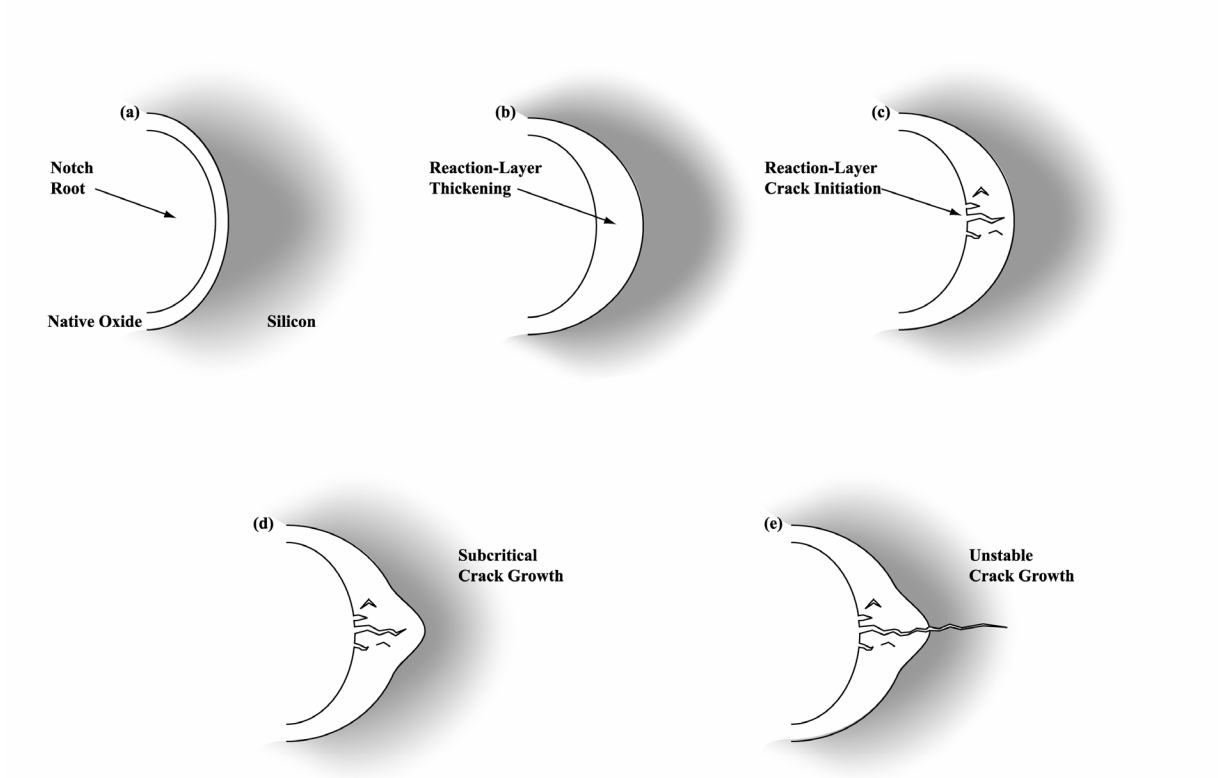

Fig. 5. Schematic illustration of the "reaction-layer fatigue" mechanism at the notch of the poly-crystalline silicon cantilever beam.

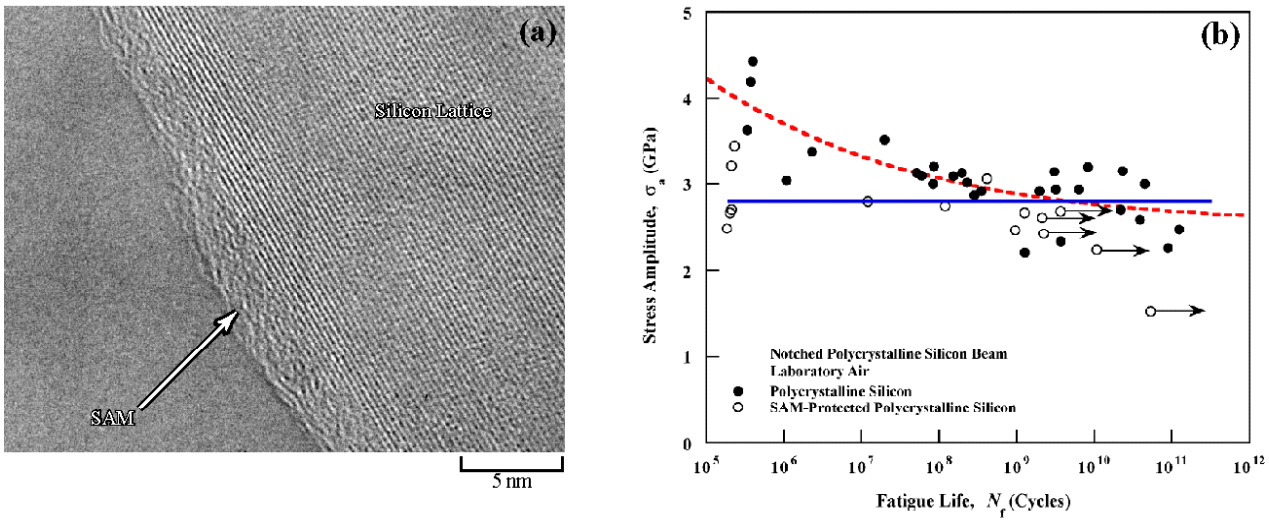

Fig. 6. (a) TEM image showing a 1-octadescene self-assembled monolayer (SAM) coating the root of the polysilicon notch; the absence of the oxide is shown by the lattice fringes of the silicon visible under the ~3 nm layer. (b) *S/N* curves showing the reduced susceptibility of such SAM-coated polysilicon films to fatigue failure.

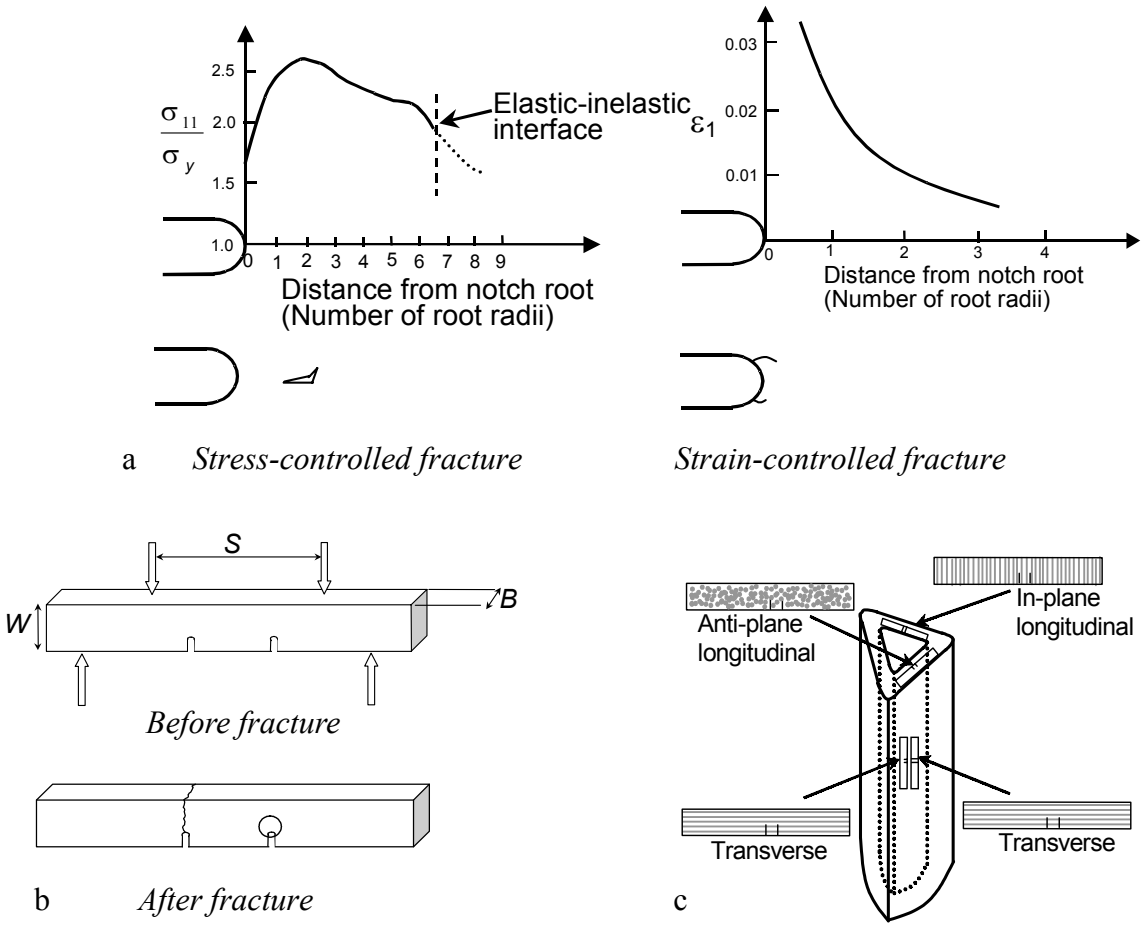

Fig. 7. (a) The stress (left) and strain (right) distributions ahead of a notch, indicating that, in the presence of inelasticity, the peak stresses are *ahead* of the notch whereas the peak strains are *at* the notch. Consequently, stress-controlled fracture will initiate ahead of the notch, whereas the initial fracture event for strain-controlled fracture will be at the notch. (b) Double-notched four-point bend test. (c) Specimen orientations taken from the humerus (relative to the direction of the osteons, indicated in grey).

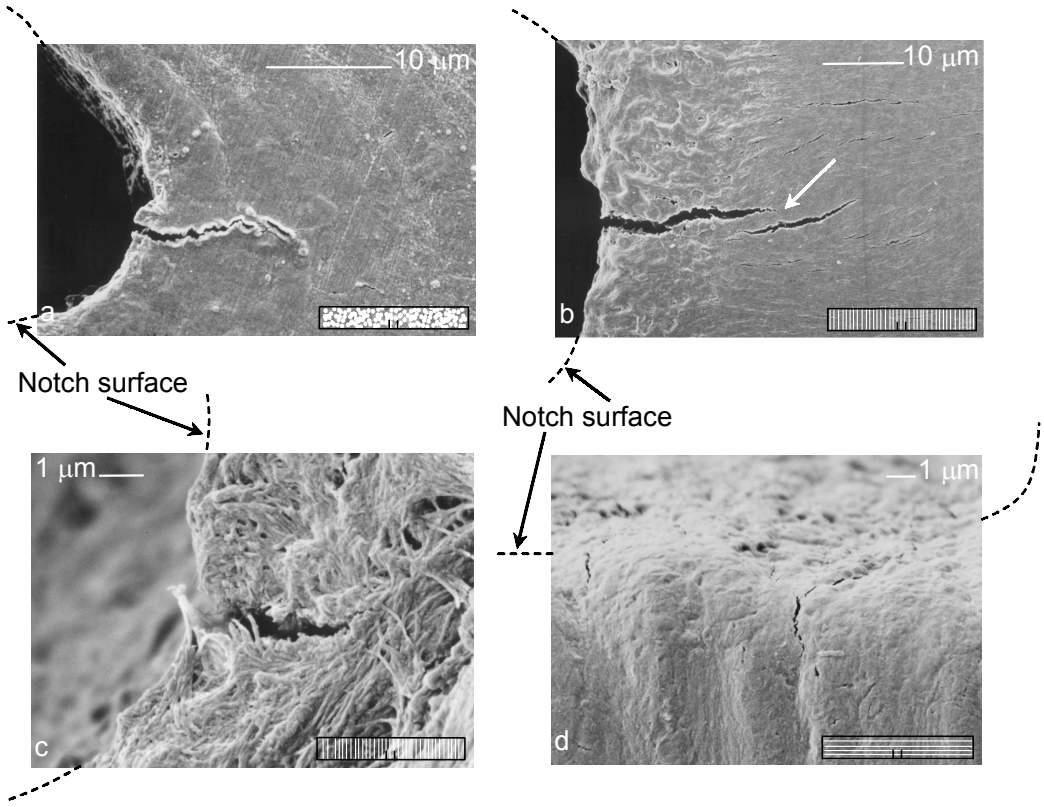

Fig. 8. SEM micrographs of the area near the unbroken notch: (a) A crack emanating directly from the notch in the anti-plane longitudinal (medial-lateral) orientation. (b) Uncracked-ligament bridging (indicated by white arrow) and microcracking for the in-plane longitudinal (proximal-distal) orientation. (c) The <5 μm size of precursor cracks shows that initiation is at the notch and not ahead of it, consistent with locally strain-controlled fracture. (d) The strong influence of microstructure leads to cracks emanating well behind the notch root in the transverse orientation. Also, multiple crack initiation can be seen. The insets show the specimen orientation with respect to the direction of the osteons.

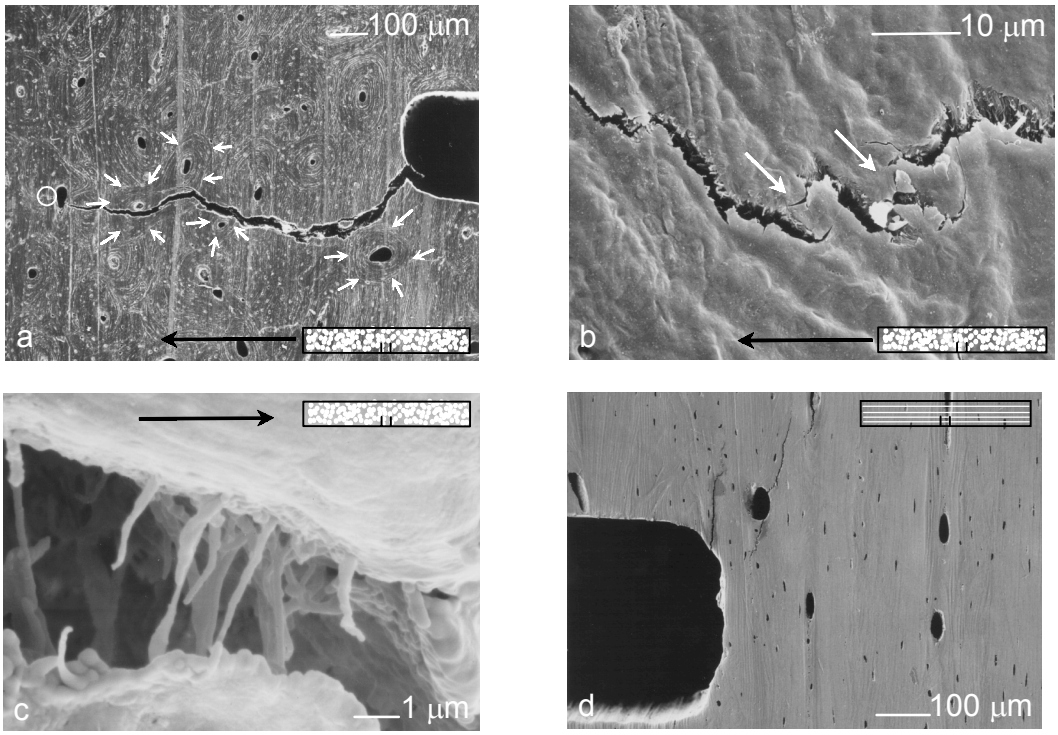

Fig. 9. SEM micrographs illustrating toughening mechanisms in bone through interactions between the crack and the microstructure: (a) For a crack emanating from the notch in the anti-plane longitudinal orientation, the crack path appears to be little influenced by the osteons (encircled by the white arrows). (b) A high magnification image of the region indicated in a by a white circle showing evidence of uncracked-ligament bridging as a contribution to the toughness (indicated by white arrows). (c) A high magnification micrograph showing crack bridging by collagen fibrils, also for anti-plane longitudinal orientation. (d) A stronger influence of microstructure is evident for the transverse orientation, where cracking ahead of the notch is shown at a Haversian canal, although the actual initiation process is at the notch itself, as evidenced by the presence of precursor cracks (Fig. 8d). The insets show the specimen orientation with respect to the direction of the osteons; the black arrows indicate the nominal direction of crack growth.

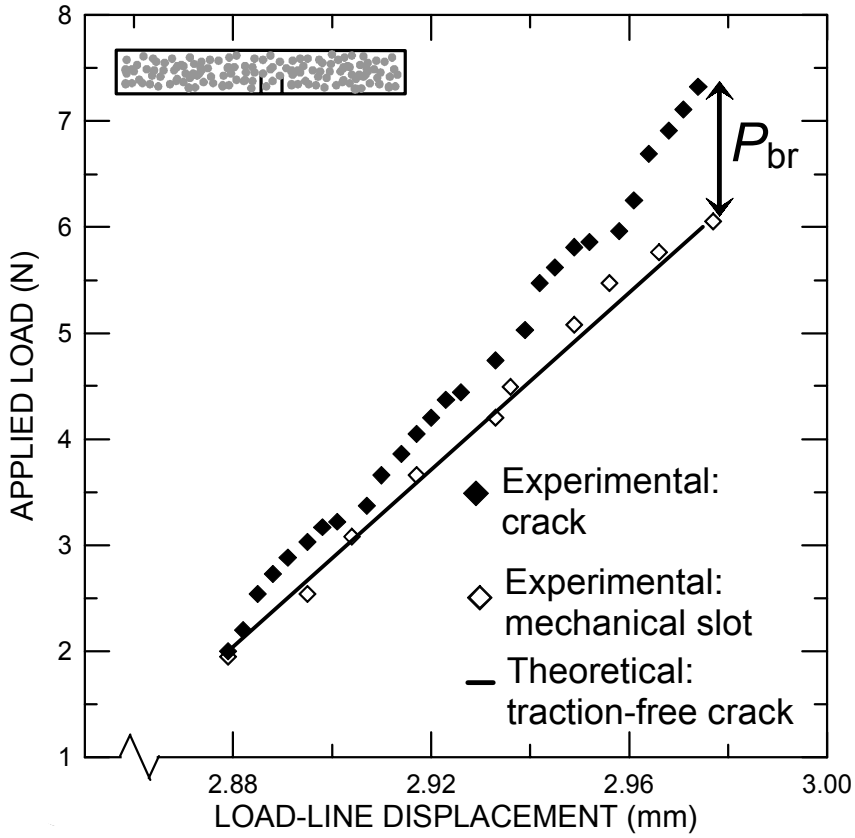

Fig. 10. Experimental (bridged) and theoretical (traction-free) load-displacement curves (at fixed crack length) for human cortical bone (anti-plane longitudinal orientation) used to assess the compliance and to verify the existence of (and quantify) the bridging levels involved.

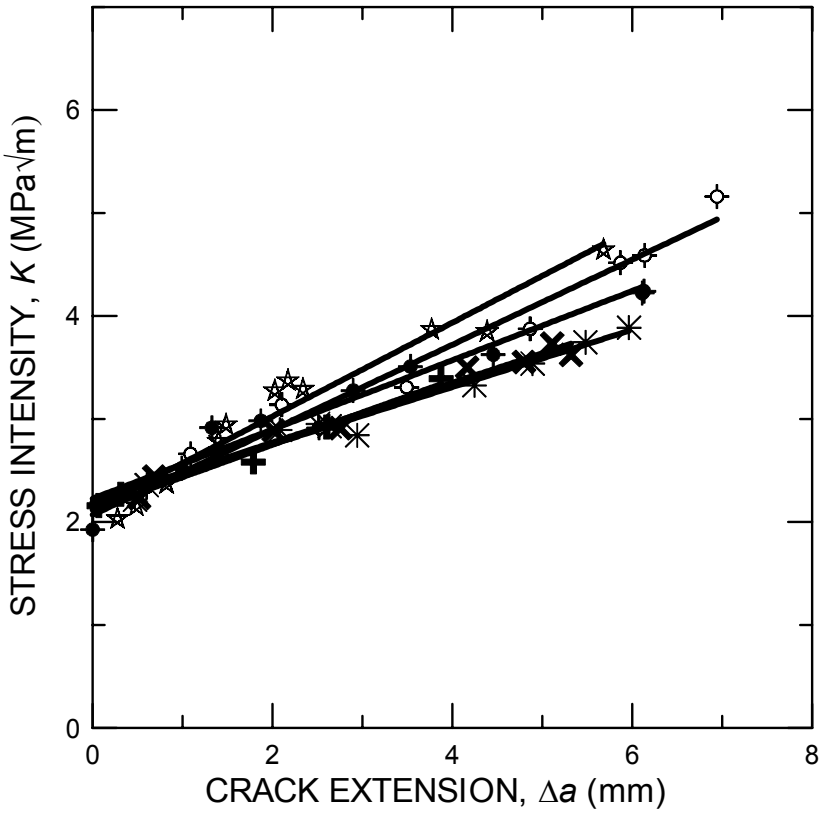

Fig. 11. $K_R(\Delta a)$ resistance-curves for stable *in vitro* crack extension in hydrated cortical bone. Note the linearly rising R-curve behavior.

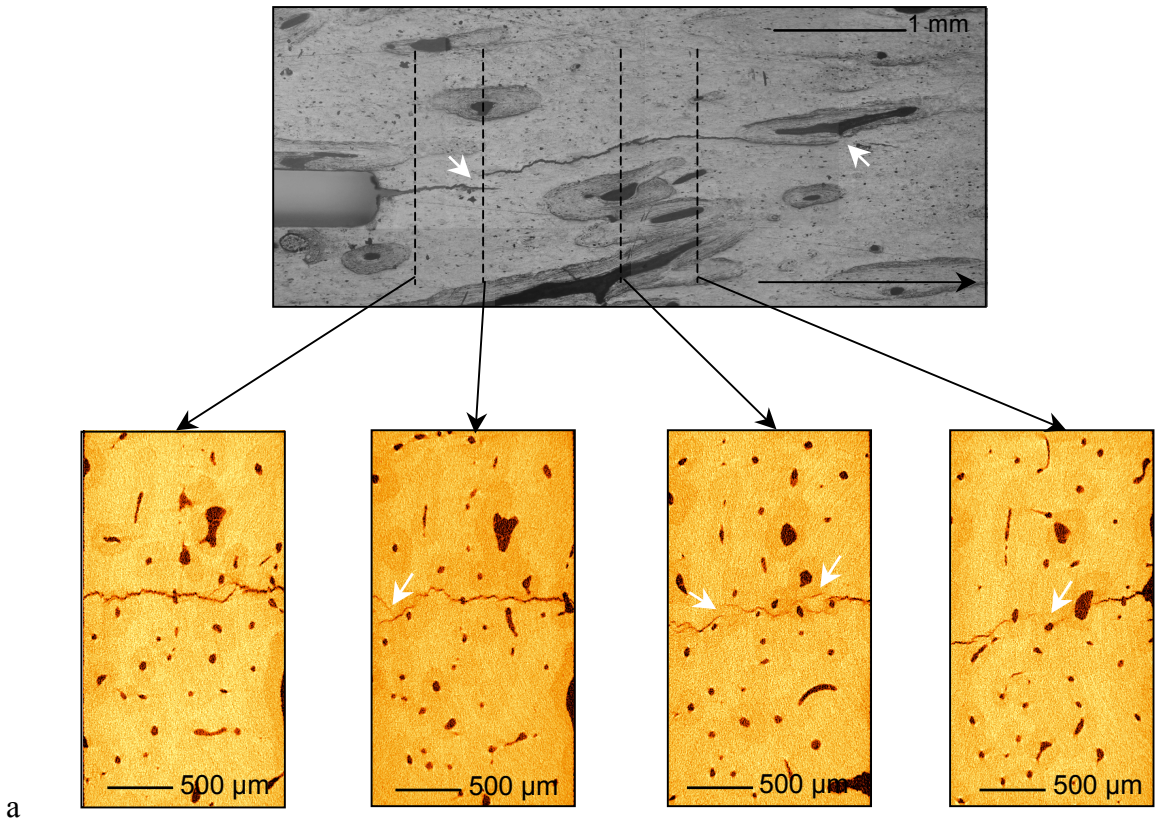

a

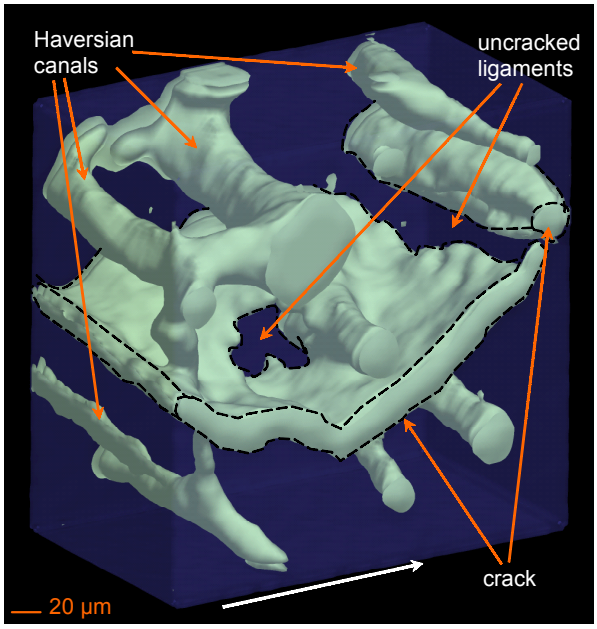

b

Fig. 12. (a) An optical micrograph (center) together with tomographic through-thickness slice-wise two-dimensional reconstructions (below) clearly support the presence of uncracked ligaments (indicated by white arrows) in the crack wake. (b) Three-dimensional tomographic reconstructions of a section of a similar crack in (a) are shown. Note that the crack appears to "ignore" the osteon. Uncracked ligaments are indicated. The white arrow in each case is the direction of nominal crack growth.